XXIst Moriond Astrophysics Meeting - Les Arcs March 10-17, 2001

RESOLVING THE X–RAY BACKGROUND WITH CHANDRA: THE 1MS OBSERVATION OF THE CHANDRA DEEP FIELD SOUTH

P.Tozzi[1], J. Bergeron[2], S. Borgani[3], R. Giacconi[4], R. Gilli[5], R. Gilmozzi[2], N. Grogin[6], G. Hasinger[7], K. Kellerman[8], L. Kewley[5], A. Koekemoer[6], V. Mainieri[2,9], M. Nonino[1], C. Norman[5], P. Rosati[2], E. Schreier[6], P. Shaver[2], G.Szokoly[7], J.X. Wang[5,10], W. Zheng[5], A. Zirm[5]

[1]*Osservatorio Astronomico di Trieste, via G.B. Tiepolo 11, I–34131, Trieste, Italy*

[2]*European Southern Observatory, Karl-Schwarzschild-Strasse 2, D-85748 Garching, Germany*

[3]*INFN, c/o Dip. di Astronomia dell'Università, via Tiepolo 11, I–34131, Trieste, Italy*

[4]*Associated Universities Inc., 1400, 16th st. NW, Washington DC 20036, USA*

[5]*Dept. of Physics and Astronomy, The Johns Hopkins University, Baltimore, MD 21218, USA*

[6]*Space Telescope Science Institute, 3700 S. Martin Drive, Baltimore, MD 21210, USA*

[7]*Astrophysikalisches Institut, An der Sternwarte 16, Potsdam 14482 Germany*

[8]*NRAO, 520 Edgemont Road, Charlottesville, Virginia*

[9]*Dip. di Fisica, Universita' degli Studi Roma Tre, Via della Vasca Navale 84, I-00146 Roma, Italy*

[10]*Center for Astrophysics, University of Science and Technology of China, Hefei, Anhui, 230026, P. R. China*

The Chandra X–ray Observatory completed a 940 ksec exposure with ACIS–I of the Chandra Deep Field South (herafter CDFS) on December 24, 2000. We review here the main findings from the X-ray analysis of this dataset. We detected 360 sources, mostly AGNs, down to limiting fluxes of 5×10^{-17} erg cm^{-2} s^{-1} in the soft 0.5–2 keV band and 4×10^{-16} erg cm^{-2} s^{-1} in the hard 2–10 keV band on a 0.1089 square degrees field. The LogN–LogS relations show the resolution of the X–ray background into point sources at the level of 83–99% in the 1–2 keV band and 65–98% in the hard 2–10 keV band, given the uncertainties in the unresolved value. The so called "spectral paradox" is solved by a hard, faint population of sources constituted mostly by nearby ($z \leq 1$) absorbed (Type II) AGNs with luminosities $L \simeq 10^{42} - 10^{44}$ erg s^{-1}. We discuss also other populations of X–ray sources detected in the CDFS, namely soft, low–luminosity normal galaxies, and some relevant extended sources.

1 Introduction

In these proceedings we review the on-going analysis of the 940 ks exposure (hereafter 1Msec) of the Chandra Deep Field South (Giacconi et al. 2001; Tozzi et al. 2001; hereafter Paper I and Paper II, Giacconi et al. 2001b, Rosati et al. 2001). We reached an on–axis flux limit of $S = 4 \times 10^{-16}$ erg s^{-1} cm^{-2} and $S = 5 \times 10^{-17}$ erg s^{-1} cm^{-2} in the hard (2–10 keV) and soft (0.5–2 keV) band respectively. This is the deepest X–ray exposure to date at the time of writing, considerably extending the published deep X–ray surveys with Chandra (Mushotzky et al. 2000; Hornschemeier et al. 2000; 2001; Brandt et al. 2000; Garmire et al. 2001) and with XMM (Hasinger et al. 2001a). A comparable exposure time will be reached in the Hubble Deep Field North by the Penn State University group.

In Figure 1 we show the color image of the field, composed by 11 exposures with different roll angles. The figure is smoothed on a 1 arcsec scale. The point spread function ranges from $\sim$1 arcsec in the very center to $\simeq 8$ arcsec in the outer regions of the detector. The color image was constructed using three cuts in energy: 0.3–1 keV, 1–2 keV, 2–7 keV. These three bands contain an approximately equal numbers of photons from the detected sources. Blue sources are totally absorbed in the soft (0.5–2 keV) band, most likely due to an intrinsic absorption from neutral hydrogen with column densities typically exceeding $N_H > 10^{22}$ cm^{-2}. Very soft sources appear red. Three extended sources stand out in the field, which have been identified as groups of galaxies at medium redshifts ($z \simeq 0.5$). It is possible to see the emergence of the hard (blue) population at faint fluxes, which resolves the so called *spectral paradox*. In fact, the spectrum of the sources detected from previous X–ray missions (namely ROSAT and ASCA) at fluxes brighter than 10^{-13} erg s^{-1} cm^{-2}, showed a spectral slope of $\Gamma \simeq 1.7-1.8$, at variance with the spectral slope of the unresolved X–ray Background in the 2–10 keV band, which is $\langle\Gamma\rangle \simeq 1.4$. It is believed that the population of sources at fluxes lower than $S = 10^{-13}$ erg s^{-1} cm^{-2} have harder spectra, in order to reproduce the observed slope of the unresolved XRB. Chandra and XMM have now made possible the direct detection of such a population, mostly composed by absorbed AGNs.

Here we summarise the results from the X–ray data alone, namely the soft and hard counts, the contribution to the X–ray background (XRB), and the X-ray spectral properties of the sample. We will also discuss in detail some relevant sources, including a population of soft, optically normal galaxies and few extended sources. The optical data and the redshifts are not discussed in these proceedings (see Paper II; Rosati et al. 2001; Giacconi et al. 2001b).

2 Observation and Data Reduction

The Chandra Deep Field South (CDFS) data presented here have been obtained by adding 11 pointings of the Chandra satellite from October 1999 to December 2000. The first two exposures were taken with the Advanced CCD Imaging Spectrometer–Imaging (ACIS–I) detector at a temperature of -110 C, while the remaining 9 at a temperature of -120 C. All the exposures were taken in the faint mode.

The data were reduced with the same technique already described in Paper I and II using the standard software developed at the Cfa (CIAO release V1.5, see http://asc.harvard.edu/cda). The data were filtered to include only the standard event grades 0,2,3,4 and 6. All hot pixels and columns were removed. We removed the flickering pixels with more than two events contiguous in time, where a single time interval was set to 3.3 s. Time intervals with background rates larger than 3 σ over the quiescent value (~ 0.31 counts s^{-1} per chip in the 0.3–10 keV band) were removed. The 11 observations give a total exposure time of 940 ks out of a total of 1Ms of observing time. The pointings had different roll angles, enabling a total coverage of 0.1089 deg^2. The exposure time across the field varies from a maximum of 940 ks in the center to a minimum of 25 ks in the corners. The area covered by 940 ks of exposure is 0.0630 deg^2. The resulting exposure map is the sum of the exposure maps of the single observations weighted by the corresponding exposure times (see Figure 2).

To detect sources we run Sextractor (Bertin & Arnouts 1996) on the 0.5–7 keV image rebinned by a factor of two, so that one image pixel corresponds to 0.984$''$. Sextractor detection parameters were chosen as a result of simulations and we adopted a detection threshold of 2.4, with a Gaussian filter with 1.5 arcsec FWHM and a minimum area of 5 pixels. Sextractor is not

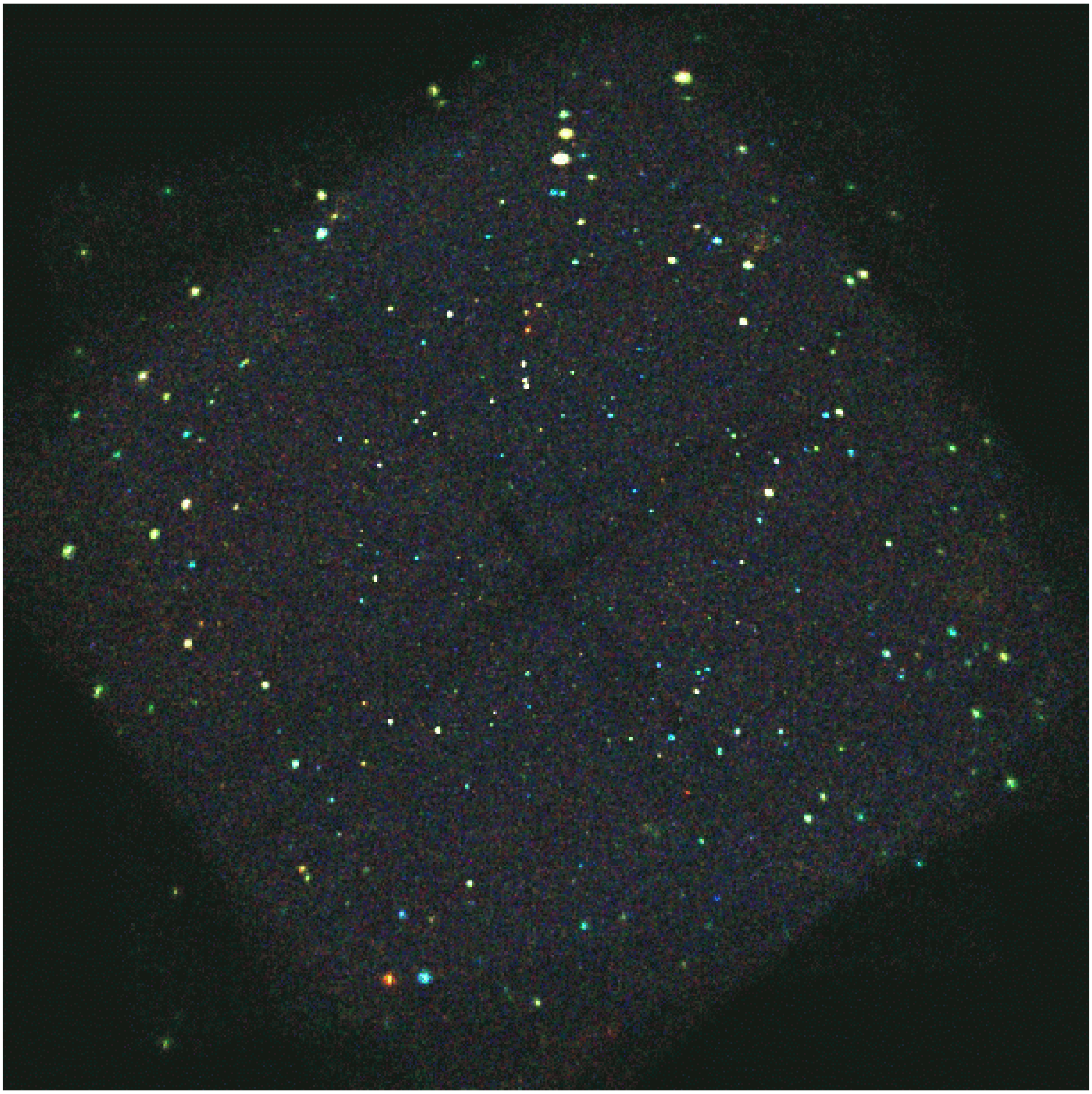

Figure 1: A color image of the 1 Ms exposure of the Chandra Deep Field South (binned 2x2, one pixel=0.984"). The image was obtained from three energy cuts: 0.3–1 keV; 1–2 keV; 2–7 keV (used respectively for red, yellow and blue). It is possible to see the emergence of the hard (blue) population at faint fluxes. The extended red spot in the center of the upper–right chip is a group of galaxies at redshift $z \simeq 0.7$. The color intensity is derived directly from the net counts and has not been corrected for vignetting (Rosati et al. 2001).

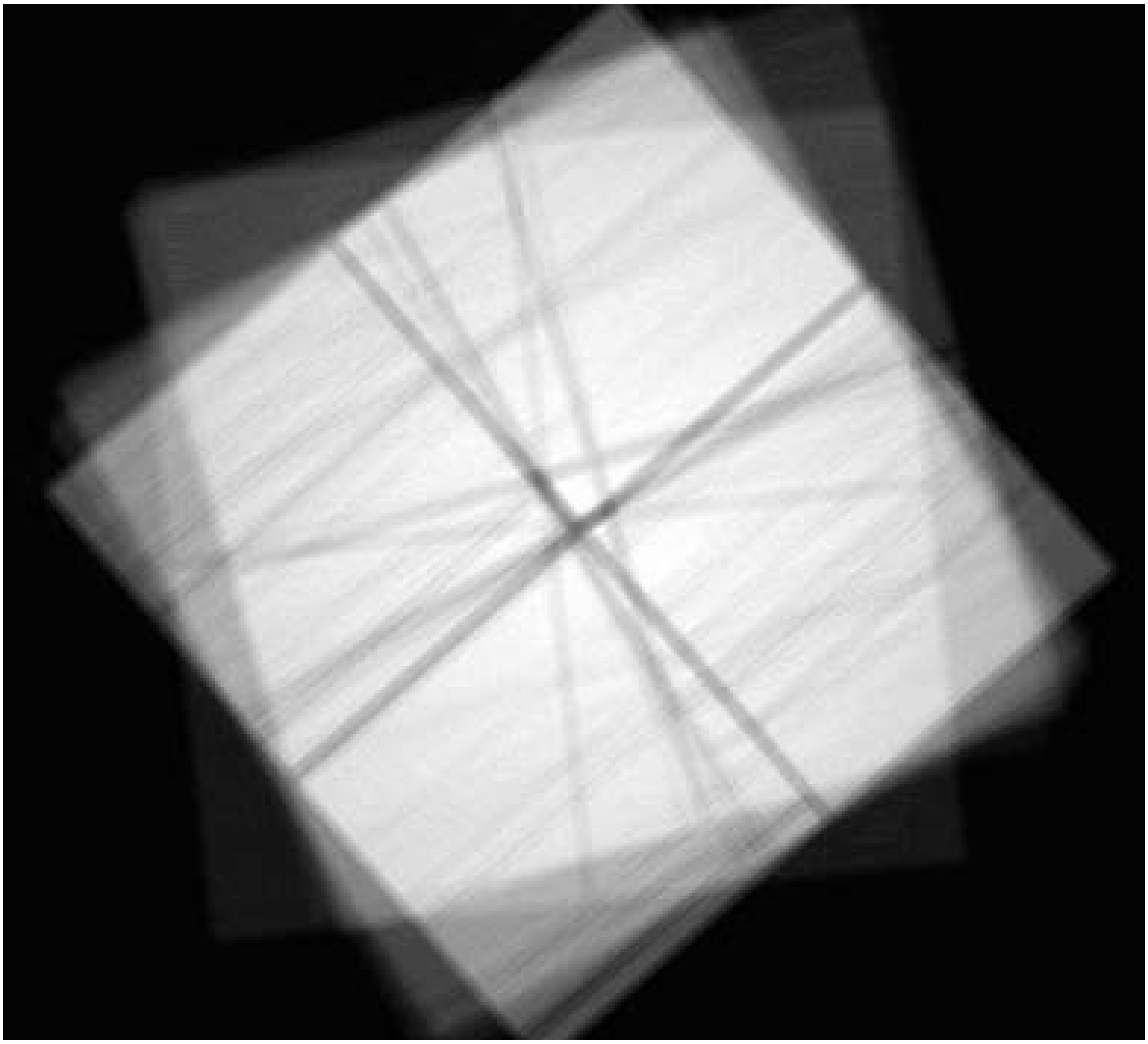

Figure 2: The exposure map computed at the energy of 1.5 keV for composite 1 Ms observation of the CDFS. The total field is 0.1089 deg^2, while the solid angle with the maximum exposure of 940 ks is 0.0630 deg^2. The crosses are the gaps between the 4 ACIS–I chips (Giacconi et al. 2001b).

tailored for use with a very low and sparse background as in ACIS–I. We used a modified version of the program to allow an external map to be used as local background. The smoothed map of the background was computed from the data itself after the removal of the sources down to a very low threshold. This modified detection algorithm is several orders of magnitude faster than the wavelet detector algorithm of Rosati et al. (1995) or WAVDETECT in the CIAO software (Freeman et al. 2001). The performance of Sextractor has been tested with simulations. We used the MARX v3.0 simulator (Wise et al. 2000) to generate the photon distribution of sources drawn from an input LogN–LogS modeled on the observed one. Our detection technique, coupled with our model for the sky coverage (see below) is able to reproduce the input number counts with accuracy of few percent. An example of such simulations is shown in Figure 1 of Paper II.

To build our catalog, we apply a signal to noise filter to the sample identified by Sextractor. We measure the signal to noise ratio of all the candidate detections in the area of extraction of each source, which is defined as a circle of radius $R_s = 2.4 \times FWHM$ (with a minimum of 5 pixels of radius). The FWHM is modeled as a function of the off-axis angle to reproduce the broadening of the PSF. In each band a detected source has a $S/N \equiv S/\sqrt{S+B} > 2.1$ within the extraction area of the image. Here B are the background counts found in an annulus with an outer radius $R_S + 12''$ and an inner radius of $R_S + 2''$, after masking out other sources, rescaled to the extraction region. Two S/N–filtered catalogs are derived from the soft and hard images. A combined catalog is then produced matching the two. We stress that the condition of having $S/N > 2.1$ in the extraction area corresponds to a high significance detection (the faintest detected sources have more than 10 counts). Our catalog now typically includes less than 5 spurious sources, as tested with simulations. Source counts are measured with simple aperture photometry within R_s in the soft and hard bands separately. Simulations have shown that such aperture photometry leads to an underestimate of the source count rate by approximately 4%. We will correct such photometric bias before converting count–rates into energy fluxes.

The energy fluxes are obtained from the observed net count–rates using a count–rate to flux conversion factors in the soft and hard bands for an average photon index $\Gamma = 1.4$ and a Galactic absorbing column of 8×10^{19} cm^{-2}. The conversion factors are $(4.6 \pm 0.1) \times 10^{-12}$ erg s^{-1} cm^{-2} per count s^{-1} in the soft band, and $(2.9 \pm 0.3) \times 10^{-11}$ erg s^{-1} cm^{-2} per count s^{-1} in the hard band. We quote the fluxes in the canonical 2–10 keV band, as extrapolated from counts measured from the 2–7 keV band, in order to have a direct comparison with previous results. The uncertainties in the conversion factors reflect the range of possible values for the effective photon index shown by the sources in our sample: $\Gamma = 1.0 - 1.8$.

The conversion factors were computed at the aimpoint. Before computing the energy fluxes, the count rates must be corrected for vignetting and are converted into the values that would have been measured if the sources were in the aimpoint. The correction is simply given by the ratio of the value of the exposure map at the aimpoint to the value of the exposure map at the source position. This is done separately for the soft and the hard band, using the exposure maps computed for energies of 1.5 keV and 4.5 keV. This procedure also accounts for the large variation in exposure time across the field of view.

3 Resolving the Soft XRB

The sky–coverage is computed with the same criteria described in Paper II. The effective sky coverage is defined as the area on the sky where a source with a given net count–rate can be detected with a $S/N > 2.1$ in the extraction region defined above. The computation includes the effect of varying exposure, vignetting and point response function across the field. Such a procedure has been tested extensively with simulations performed with MARX v3.0, and it has been shown to be accurate to within a few percent. The sky coverage is given in Figure 3 for the soft and hard bands. The sharp decrease at low fluxes determines our flux limit in the

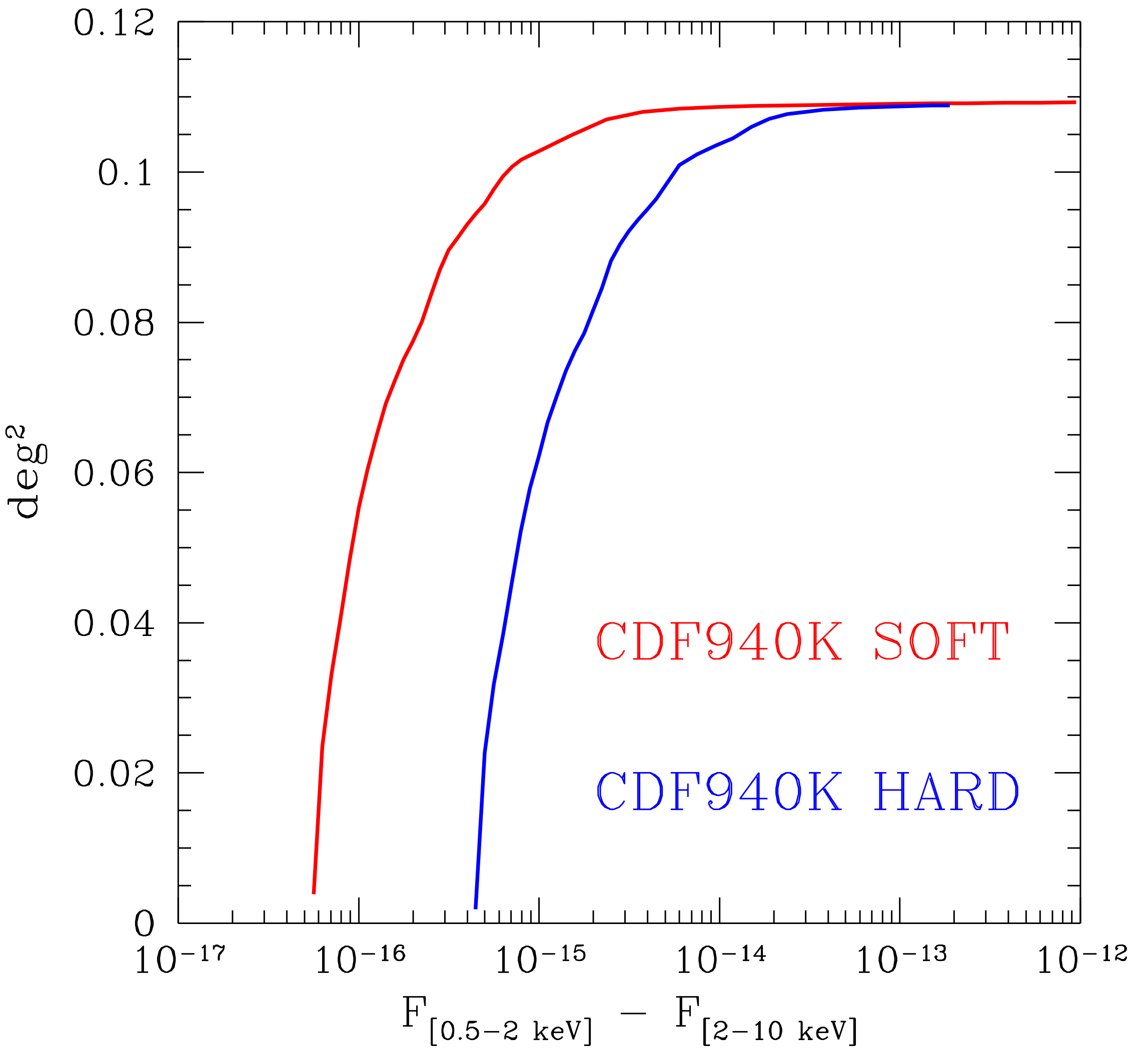

Figure 3: Sky coverage of the 1 Ms exposure of the Chandra Deep Field South for the soft (red line) and the hard (blue line) bands, as a function of the soft and hard fluxes respectively (Tozzi et al. 2001, Rosati et al. 2001).

corresponding band.

Using the sky–coverage we can compute the number counts in the soft and hard bands. In the soft band the Chandra data extend the results from previous surveys down to 5×10^{-17} erg s^{-1} cm^{-2}, covering about 3 orders of magnitude in flux (see Figure 4). The clear flattening with respect to the bright counts by ROSAT ($S > 10^{-13}$ erg s^{-1} cm^{-2}) shown in Paper I and II (also found by Mushotzky et al. 2000) is confirmed. To check if the number counts are flattening in the investigated flux range, we perform a fit with a double power law for the differential number counts. The fit is done on 4 parameters: faint–end normalization and slope, bright–end slope and flux where the break occurs. We find that the differential counts are well fitted by a power law which is consistent with the euclidean slope at the bright end and with a slope $\alpha_{diff} \equiv \alpha + 1 = 1.63 \pm 0.13$ (1 sigma) at the faint end, with a break at $S = 1.5 \times 10^{-14}$ erg s^{-1} cm^{-2}. Thus, below $S = 10^{-15}$ erg s^{-1} cm^{-2}, the slope of the cumulative number counts is $\alpha \simeq 0.6$. This represents a significant flattening with respect to the single power–law fit done in Paper I on a smaller flux range (see inset in Figure 4).

We compared our LogN–LogS with the predictions of the AGN population synthesis models described in Gilli, Salvati & Hasinger (2001). We consider their model B, where the number ratio R between absorbed and unabsorbed AGNs is assumed to increase with redshift from 4, the value measured in the local Universe, to 10 at $z \sim 1.3$, where R is unknown. This model was found to provide a better description of the X–ray constraints with respect to a standard model where R=4 at all redshifts. The value of R was independent of the luminosity and therefore a large population of obscured QSOs is included in the model. Such a model was originally calibrated to fit the background intensity measured by ASCA. The parameters of the AGN X–ray luminosity functions assumed in the model B are recalibrated to fit the background intensity measured by HEAO–1. The predictions for the source counts (short dashed line in Figure 4) are in very good agreement with the Chandra LogN–LogS at all fluxes.

For the total contribution to the soft X–ray background, we refer to the 1–2 keV band, following Hasinger et al. (1993; 1998) and Mushotzky et al. (2000). In this energy band the comparison with the unresolved soft X–ray background is more straightforward than in the 0.5–2 keV band, since for energies < 1 keV the Galactic contribution may be significant. The unresolved value in the 1–2 keV band measured by ROSAT is 4.4×10^{-12} erg s^{-1} cm^{-2}, while the value found by ASCA is 3.7×10^{-12} erg s^{-1} cm^{-2} (see Hasinger et al. 1998 and references therein). We find a contribution of $\simeq 6.25 \times 10^{-13}$ erg s^{-1} cm^{-2} deg^{-2} for fluxes lower than 10^{-15} erg s^{-1} cm^{-2}, corresponding to $\simeq 14-17\%$ of the unresolved flux. If this value is summed to the contribution at higher fluxes (3.02×10^{-12} erg s^{-1} cm^{-2} deg^{-2}, see Hasinger et al. 1998), we end up with a total contribution of $\simeq 3.65 \times 10^{-12}$ erg s^{-1} cm^{-2} deg^{-2} for fluxes larger than 3×10^{-17} erg s^{-1} cm^{-2} (which is our flux limit in the 1–2 keV band), corresponding to 83% of the unresolved value as measured by ROSAT. If we assume the unresolved value measured by ASCA (which must be considered as a lower limit) the resolved contribution amounts to 99%.

4 Resolving the Hard XRB

The LogN–LogS distribution for sources in the hard band is extended down to a flux limit of 4×10^{-16} erg s^{-1} cm^{-2}. The hard counts are normalized at the bright end with the ASCA data by Della Ceca et al. (1999b). We used a conversion factor for an average power law $\Gamma = 1.4$, in agreement with the average spectral shape of our total sample. We repeat the fit with a double power law in the differential counts, as in the case of the soft counts. For the hard counts too, we find evidence for further flattening: the differential counts are well fitted by a power law which is consistent with the euclidean slope at the bright end and with a slope $\alpha_{diff} = 1.58 \pm 0.12$ (1 sigma) at the faint end, with a break at $S = 8.4 \times 10^{-15}$ erg s^{-1} cm^{-2}. As in the soft case, this shows a substantial flattening with respect to the single power law fit of Paper I and of

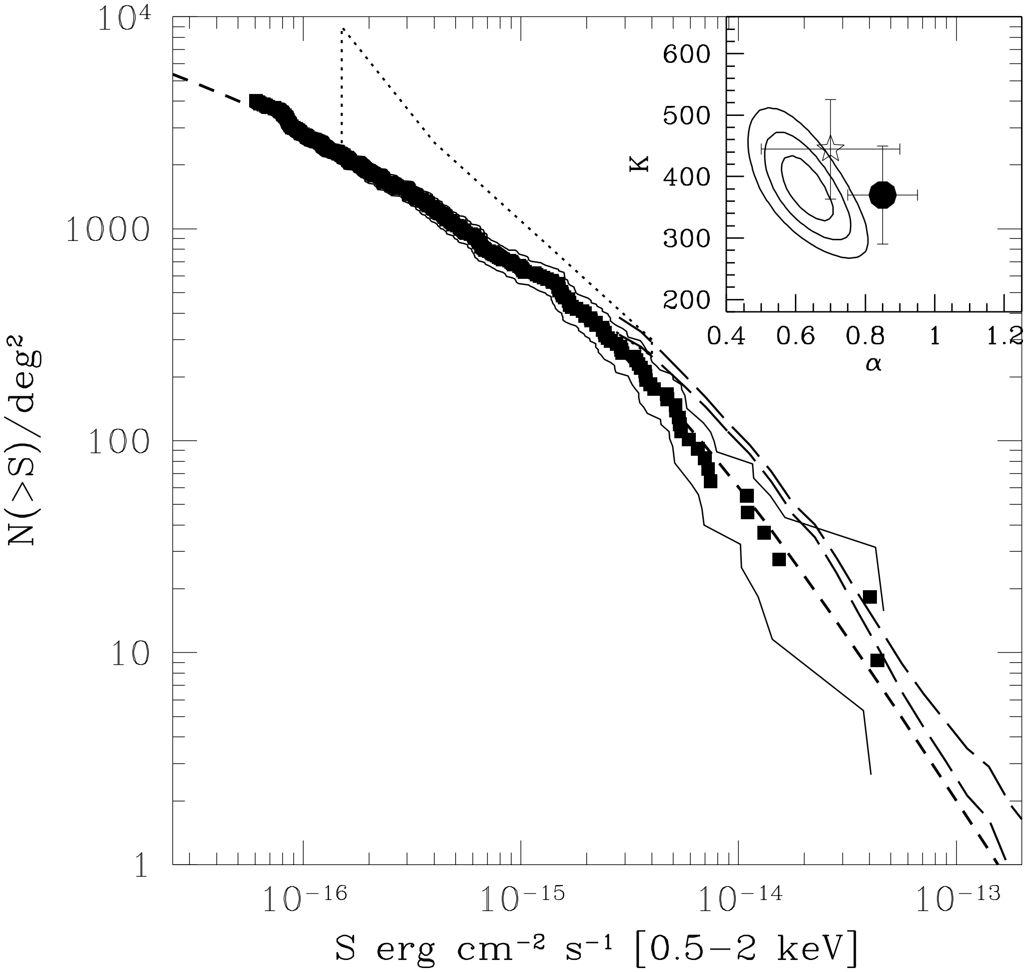

Figure 4: The LogN–LogS in the soft band from the CDFS for an average spectral slope $\Gamma = 1.4$ (filled squares, Rosati et al. 2001). Dashed lines are the counts from the Lockman Hole (Hasinger et al. 1998), and the dotted contour is the extrapolation from the fluctuation analysis in ROSAT data (Hasinger et al. 1993). The upper and lower solid lines indicate uncertainties due to the sum of the Poisson noise (1 sigma) including the uncertainty in the conversion factor. The short dashed line is from model B in Gilli, Salvati & Hasinger (2001), rescaled to fit the total background measured by HEAO–1 (see text). The insert shows the maximum likelihood contours to the slope and normalization of the faint end of the number counts from the double power law fit (the normalization is defined at $S = 2 \times 10^{-15}$ erg s^{-1} cm^{-2}). The contours correspond to 1σ, 2σ and 3σ. The star is the single power law fit from Mushotzky et al. (2000) at $S = 2 \times 10^{-15}$ erg s^{-1} cm^{-2}; the error bar is their quoted 68% confidence level. The large dot is the single power law fit from Paper I.

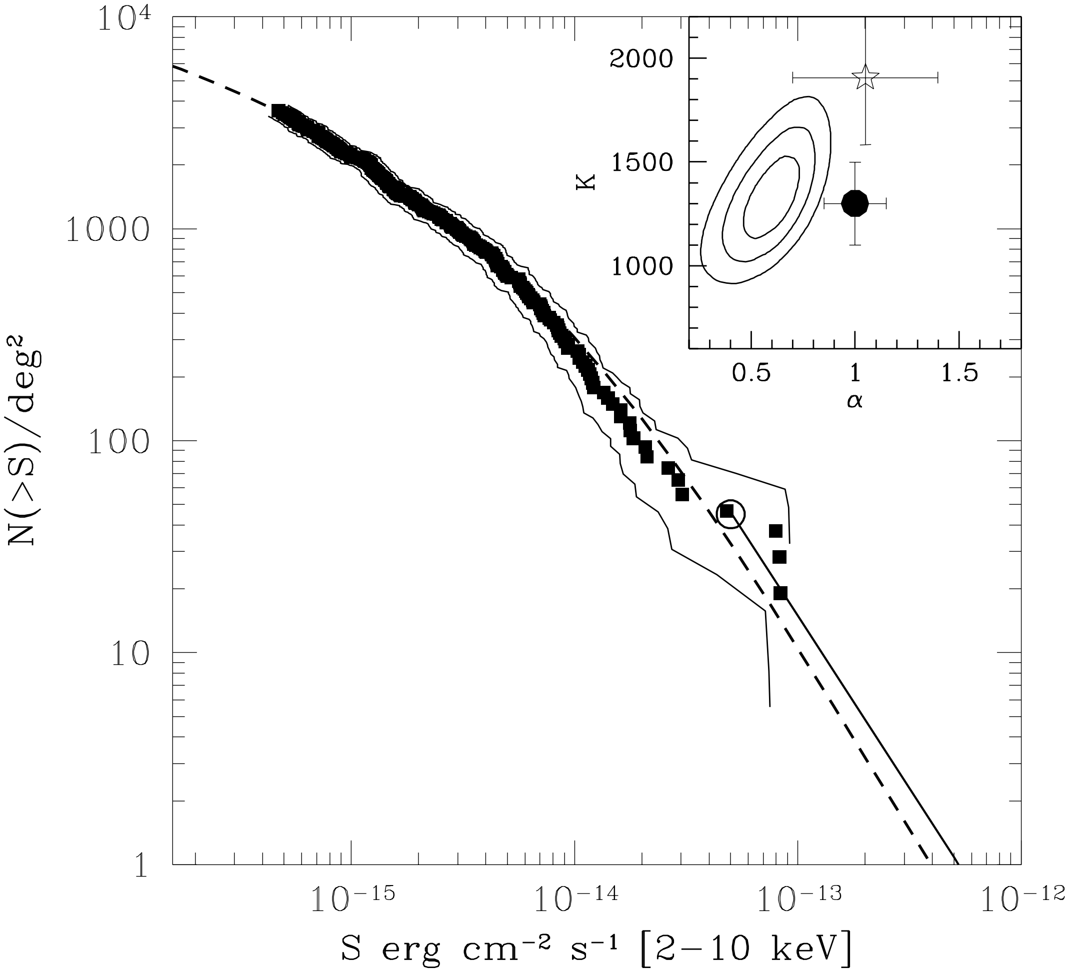

Figure 5: The LogN–LogS in the hard band from the Chandra Deep Field for an average spectral slope $\Gamma = 1.4$, symbols as in Figure 4 (Rosati et al. 2001). The open circle at high fluxes is from ASCA and Beppo SAX (Giommi, Perri & Fiore 2000; Ueda et al. 1999) and the continuous line is the fit to the counts from ASCA in the range $10^{-12} - 10^{-13}$ erg cm^{-2} s^{-1} (Della Ceca et al. 1999b). The upper and lower solid lines indicate uncertainties due to the sum of the Poisson noise (1 σ) including the uncertainty in the conversion factor. The short–dashed line is the same model of Figure 4. The insert shows the maximum likelihood contours to the slope and normalization of the faint end of the number counts from the double power law fit (the normalization is defined at $S = 2 \times 10^{-15}$ erg s^{-1} cm^{-2}). The contours correspond to 1σ, 2σ and 3σ. The star is the single power law fit from Mushotzky et al. (2000) and the error bar is their quoted 68% confidence level. The large dot is the single power law fit from Paper I.

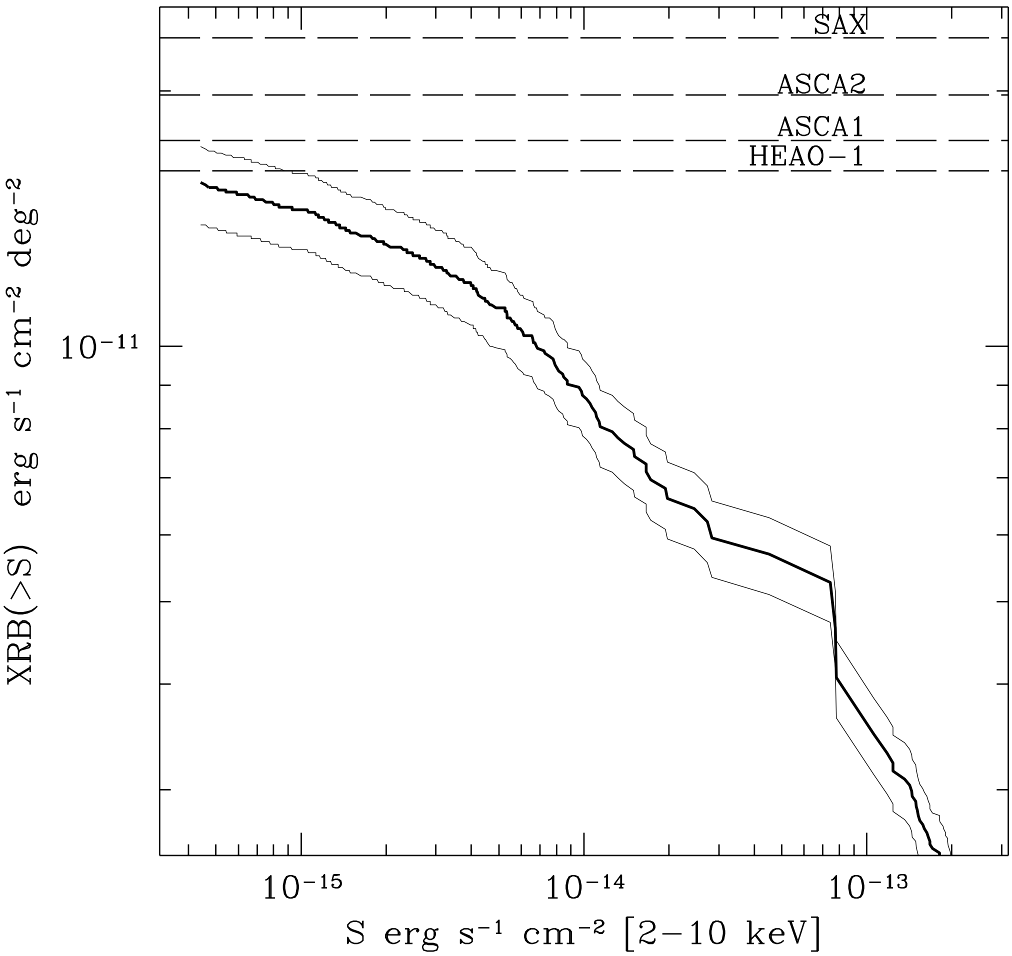

Figure 6: The contribution to the hard X–ray flux density as a function of the flux of the resolved sources (see Rosati et al. 2001). The total resolved contribution is computed from the 1 Ms CDFS sample plus the bright sample from ASCA at fluxes larger than $\simeq 10^{-13}$ erg s^{-1} cm^{-2} (Della Ceca et al. 1999b). The upper dashed lines refer to previous measures of the hard X–ray background; from bottom to top: Marshall et al. (1980, HEAO-1), Ueda et al. (1999, ASCA1), Ishisaki (1999, ASCA2), Vecchi et al. (1999, BeppoSAX).

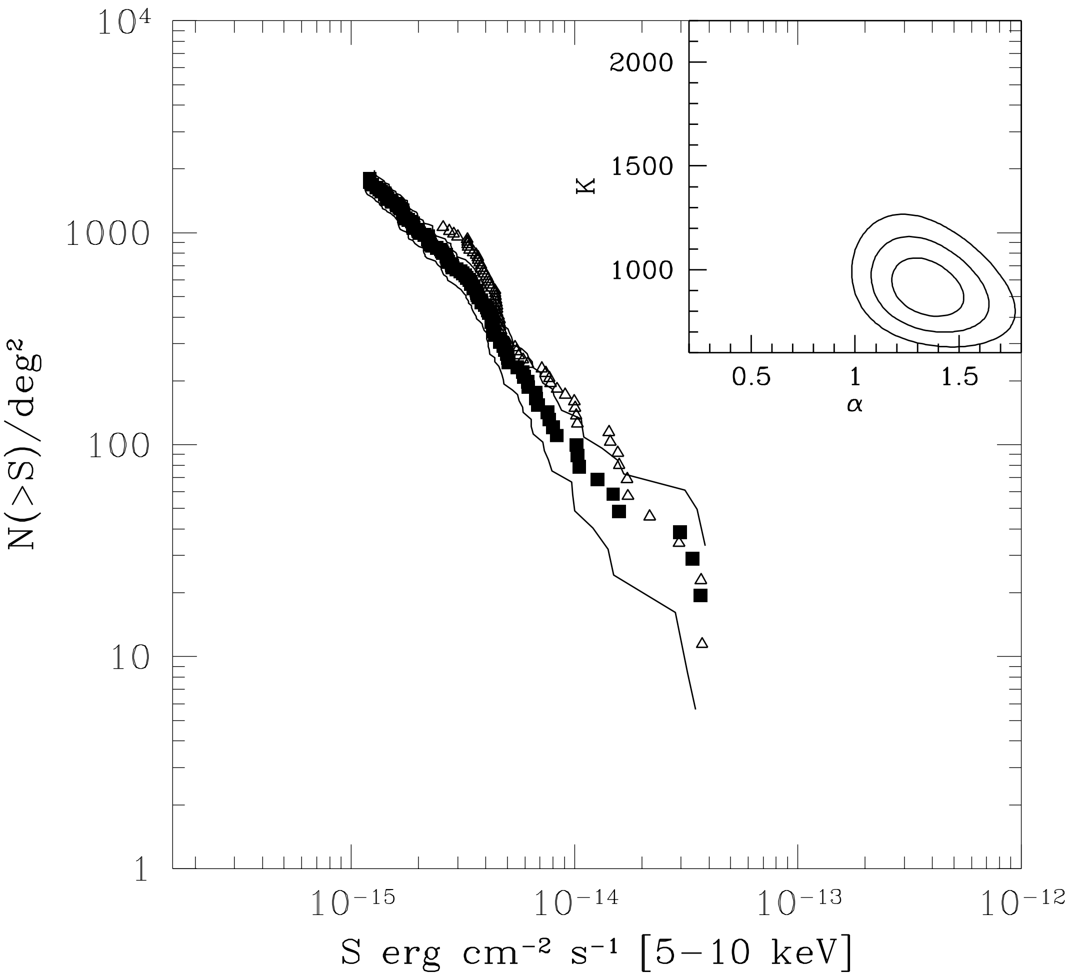

Figure 7: The LogN–LogS in the very hard band (5-10 keV) from the Chandra Deep Field for an average spectral slope $\Gamma = 1.4$ (Rosati et al. 2001). Triangles are from the XMM Deep Expsoure of the Lockman Hole (Hasinger et al. 2001). The upper and lower solid lines indicate uncertainties due to the sum of the Poisson noise (1 σ) including the uncertainty in the conversion factor. The insert shows the maximum likelihood fit to the parameters in the LogN–LogS fit. The thick contours correspond to 1σ, 2σ and 3σ.

Mushotzky et al. (2000).

The normalization K (computed at 2×10^{-15} erg s^{-1} cm^{-2}) is still at more than 3 sigma from the results of Mushotzky et al. (2000, large star in the inset of Figure 5). Our hard number counts are confirmed also by the results from the Lynx field (Stern et al. 2001) and from the XMM observation of the Lockman Hole (Hasinger et al. 2001a). The disagreement between us and Mushotzky et al. (2000) is statistically significant and acquires particular relevance since we are about to resolve completely the hard background. The causes of discrepancy may be due to calibration problems[a]. A possible physical reason is cosmic variance or clustering (the latter has been measured from the first observations of the CDFS in Paper I). In this case the larger area of the CDFS should give a more accurate measure, if compared with the smaller area (1/4) covered by the pointing of Mushotzky et al. (2000).

The integrated contribution of all the sources within the flux range 10^{-13} erg s^{-1} cm^{-2} to 4×10^{-16} erg s^{-1} cm^{-2} in the 2–10 keV band is $(1.31 \pm 0.20) \times 10^{-11}$ erg s^{-1} cm^{-2} deg^{-2} for $\Gamma = 1.4$. After including the bright end seen by ASCA for $S > 10^{-13}$ erg s^{-1} cm^{-2} (Della Ceca et al. 1999b), the total resolved hard X–ray background amounts to $(1.56 \pm 0.16) \times 10^{-11}$ erg s^{-1} cm^{-2} deg^{-2}. The inclusion of the ASCA data at bright fluxes minimizes the effect of cosmic variance. In Figure 6 we show the total contribution computed from the CDFS plus ASCA sample. The value at the limiting flux $S = 4 \times 10^{-16}$ erg s^{-1} cm^{-2} has now reached the value of the total (unresolved) X–ray background 1.6×10^{-11} erg s^{-1} cm^{-2} deg^{-2} from UHURU and HEAO-1 (Marshall et al. 1980). More recent values of the 2–10 keV integrated flux from the BeppoSAX and ASCA surveys (e.g., Vecchi et al. 1999; Ishisaki et al. 1999 and Gendreau et al. 1995) appear higher by 20-40%. Thus a fraction between 0.98 and 0.65 of the unresolved value has now been resolved into discrete sources.

We also computed the logN–logS in the very hard band (5–10 keV). As we said above, the energy range effective for detection is only 5–7 keV. In this narrow energy range, the effective area of Chandra is much lower than the one of XMM. This could be the reason of the lower normalization with respect to the very hard number counts from the deep exposure of XMM in the Lockman Hole (Hasinger et al. 2001a) as shown in Figure 7. Nevertheless, the steep slope of the very hard number counts ($\alpha \sim 1.4 \pm 0.2$) is confirmed down to $S \sim 10^{-15}$ erg s^{-1} cm^{-2}. The XMM observation of the CDFS, planned for mid 2001, will be crucial to investigate the population of very hard sources that could have been missed by Chandra. These sources are expected to be constituted by strongly absorbed, low redshift AGN.

5 Spectral Properties of X–ray Sources

We have analysed the stacked spectrum of the 360 sources of the total sample. The background was constructed using the stacked spectrum of all the background regions extracted around each source. The resulting photon files were scaled by the ratio of the total area of extraction of the sources and the corresponding area used for the background. Such a procedure guarantees a correct background subtraction despite the non–uniformities of the instrumental background across ACIS–I. The response matrices for the stacked spectra were obtained from the counts–weighted average of the matrices of each single sources. Each response matrix is composed of the sum of the matrices corresponding to that source in each single exposure, weighted by the corresponding exposure time. The same is done for the ancillary response matrices. In this way, we keep track in the most detailed way of the characteristics of the different regions and the different detector temperatures at the time of the observations. We used XSPEC v11.0 to compute the slope of a power law spectrum with Galactic absorption, in the energy range 1–9 keV. We exclude energy bins below 1 keV because the calibration is still uncertain below this

[a]A 15% underestimation of the effective area of the BI chips has been recently discovered, but only below 1.2 keV, see http://asc.harvard.edu/ciao/caveats/effacal.html)

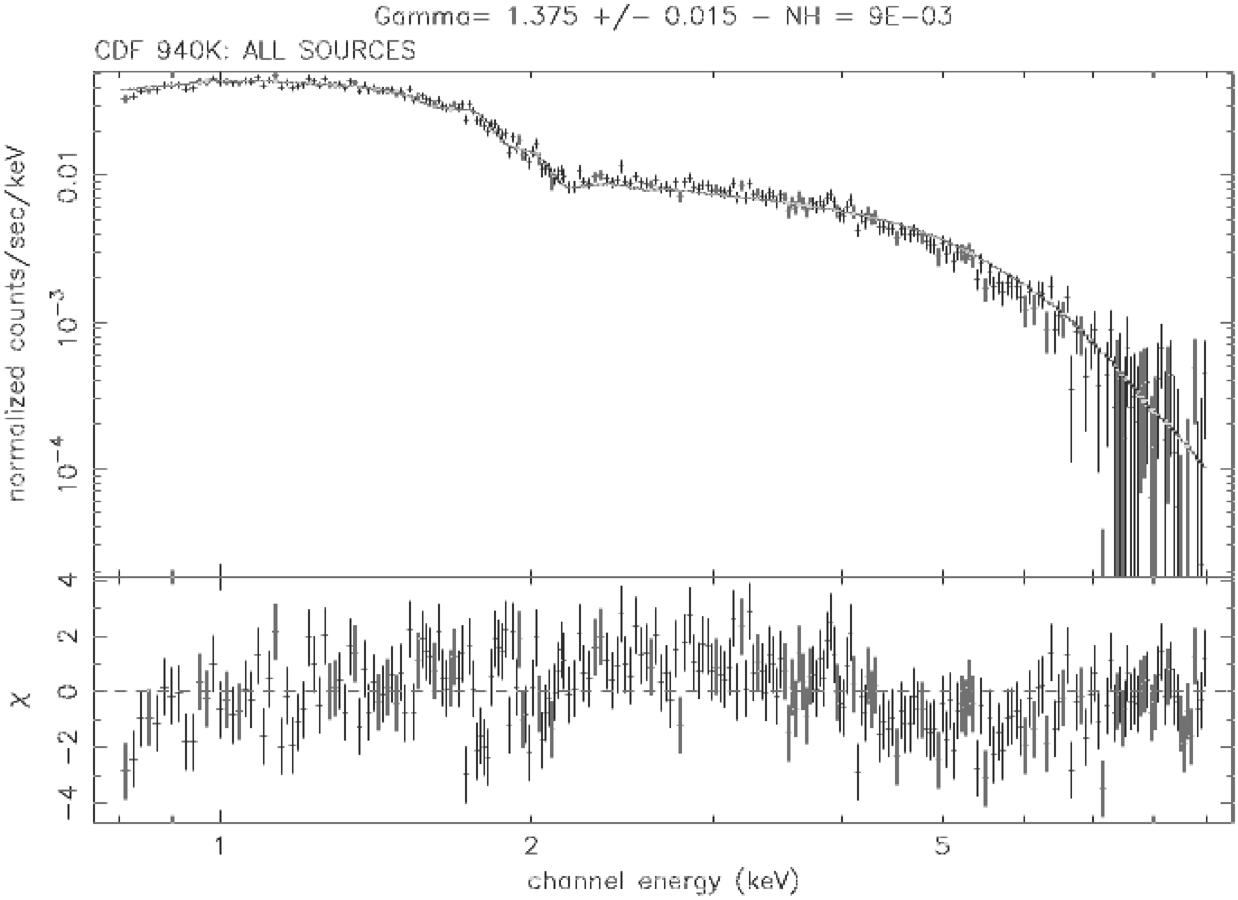

Figure 8: Stacked spectrum of the total sample of sources in the CDFS, fitted in the energy band 1–9 keV with an absorbed power law with column density fixed to the Galactic value $N_H = 8 \times 10^{19}$ cm^{-2}. The best fit slope is $\Gamma = 1.375 \pm 0.015$ (error at 90% c.l.) for a $\chi^2_\nu = 1.65$, in agreement with the average slope of the unresolved hard X–ray background. The solid line is the best–fit model, while the lower panel shows the standard deviations in each energy bin.

energy. Such uncertainty has a small effect on the average conversion factor, but can give wrong results on detailed fits. For a column density fixed to the Galactic value $N_H = 8 \times 10^{19}$ cm^{-2}, we obtained a photon index $\Gamma = 1.375 \pm 0.015$ (errors refer to the 90% confidence level) with $\chi^2_\nu = 1.65$. The results of the spectral fit to the total sample of sources are shown in Figure 8. The average spectrum of the detected sources is consistent with the measured shape of the unresolved hard background $\langle\Gamma\rangle \simeq 1.4$, confirming previous findings. However, we notice that the slope is somewhat harder than the one measured in Paper I and II, showing that we are still discovering harder sources at lower fluxes, as suggested by the steep slope of the very–hard counts.

A more detailed view of the spectral properties as a function of the fluxes comes from the hardness ratio $HR = (H - S)/(H + S)$ where H and S are the net counts in the hard (2–7 keV) and the soft band (0.5–2 keV), respectively. In both bands, the number of hard sources increases at lower fluxes (see Figure 9). To investigate the behaviour of the spectral shape as a function of the hard flux, we divided the sample of sources detected in the hard band in 4 subsamples: bright ($S > 2 \times 10^{-14}$ erg s^{-1} cm^{-2}), medium ($2 \times 10^{-14} > S > 6 \times 10^{-15}$ erg s^{-1} cm^{-2}), faint ($S < 6 \times 10^{-15}$ erg s^{-1} cm^{-2}), and very faint ($S < 2 \times 10^{-15}$ erg s^{-1} cm^{-2}). The average slope of the stacked spectra is 1.68 ± 0.03, 1.42 ± 0.03, 1.10 ± 0.03, and 1.05 ± 0.05 respectively. The trend is shown in Figure 10 together with the result from the 300 ks exposure (Paper II). Thus

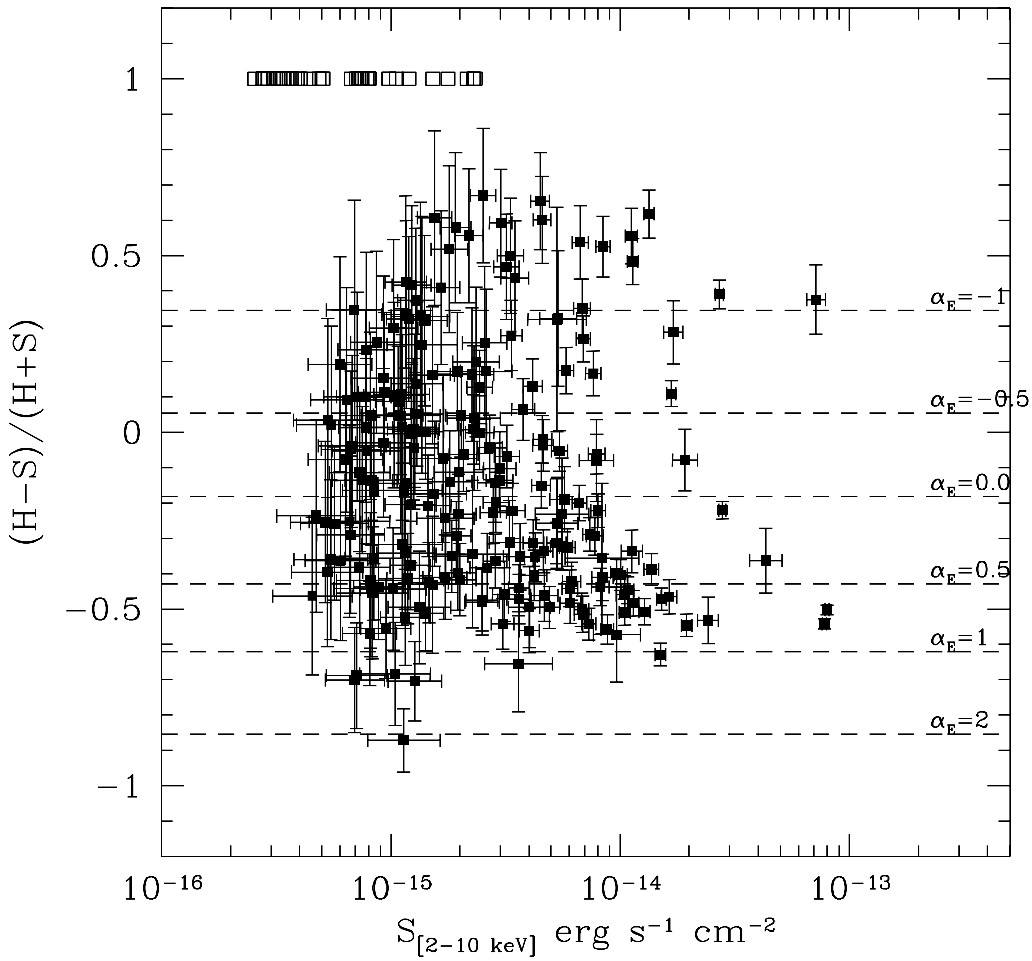

Figure 9: Hardness ratio for the sources detected in the hard image as a function of the flux. Sources detected only in the hard band are shown with open squares at HR= 1. Dashed lines are power–law models with different energy index (α_E) computed assuming the Galactic value $N_H = 8 \times 10^{19}$ cm^{-2} and convoluted with a mean ACIS–I response matrix at the aimpoint. The number of hard sources clearly increases at low fluxes.

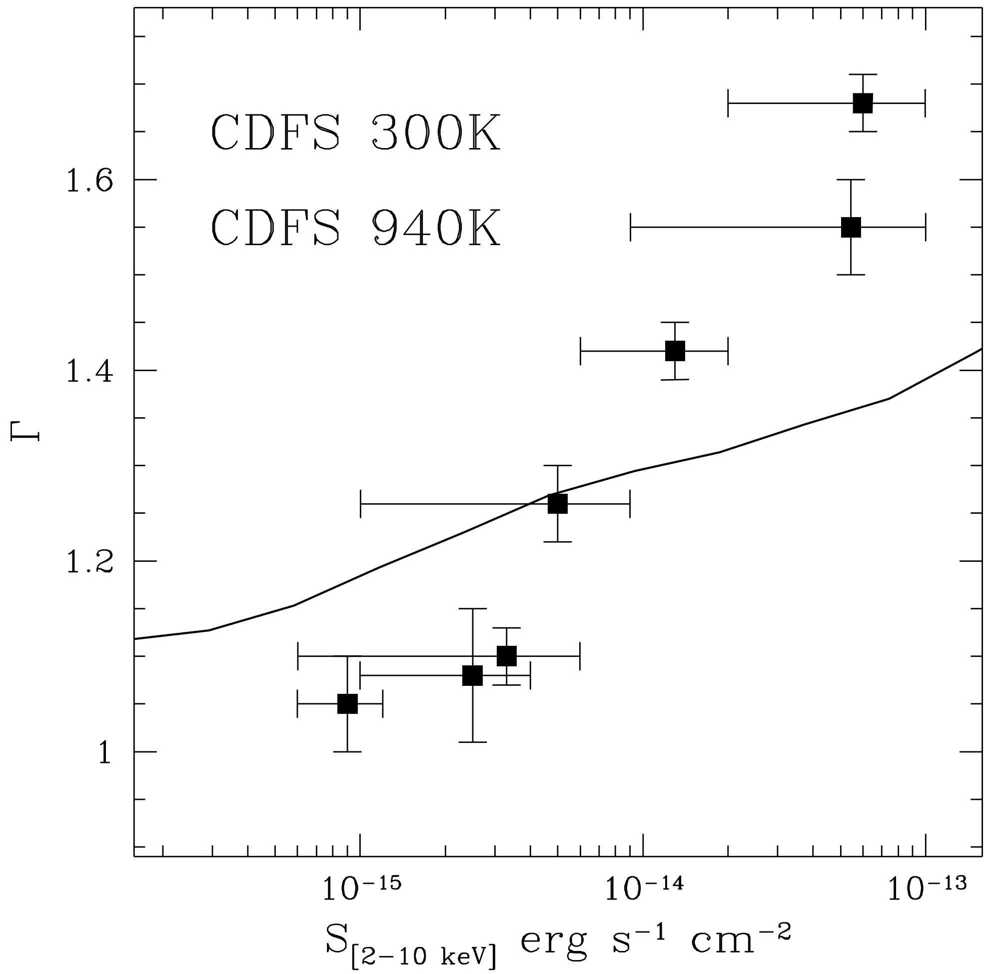

Figure 10: The average power law index of the stacked spectra of the bright, medium, faint and very faint subsamples of the sources detected in the hard band, as defined in the text. Errors on Γ refer to the 90% confidence level. The local absorption has been fixed to the Galactic value $N_H = 8 \times 10^{19}$ cm^{-2}. The line is derived from the same model of Figure 4 and 5. The green points refer to the 300 ks exposure (Paper I), while the red points to the 1Ms exposure.

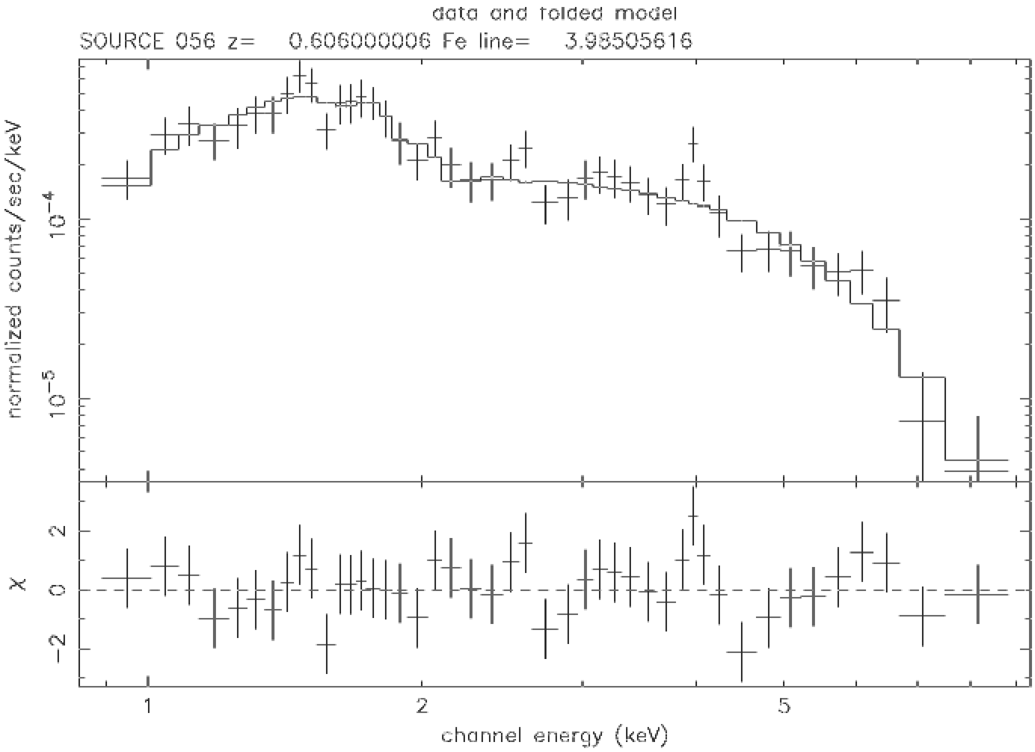

Figure 11: Spectrum of source 56 in the CDFS, folded with the response function of the instrument averaged over the 11 exposures in the position of the source. This is an example of the relatively nearby ($z = 0.606$ in this case), absorbed sources that make up the hard X–ray background, solving the spectral paradox. The intrinsic absorbing column is $N_H = (1.8 \pm 0.4)\ 10^{22}\ \mathrm{cm}^{-2}$.

we continue to detect a significant hardening of the average spectral slope at lower fluxes.

For the source detected only in the hard band, the hardness ratio of the cumulative spectrum is $HR \simeq 0.64 \pm 0.09$. The fit with an unabsorbed power law gives $\Gamma = 0.0 \pm 0.2$, but with $\chi^2_\nu \simeq 2$. This indicates that a single power law is a bad fit. If we leave the local absorption free, we obtain a better fit with $N_H = (2.5 \pm 0.5) \times 10^{22}\ \mathrm{cm}^{-2}$, which is more than two orders of magnitude larger than the Galactic value, and a power law of $\Gamma = 1.55 \pm 0.3$ (errors correspond to the 90% confidence level). Such level of absorption correspond to $N_H > 10^{23}\ \mathrm{cm}^{-2}$ for $z > 1$. This results shows that the progessive hardening of the sources at faint fluxes is probably due to intrinsic absorption.

Moreover, the average hardness ratios derived for the two subsamples tell us that the average spectrum of the sources undetected in one of the two bands is similar to that of the other sources detected in both bands at low fluxes. In other words, we expect to detect most of them in both bands in a longer exposure. The average number of soft and hard counts for the sources detected in the hard or in the soft band only, is 3.8 and 4.1 respectively (corresponding to a count rate of $\simeq 1.3 \times 10^{-5}$ cts/s). The flux where the whole sample is detected in both the soft and the hard band will depend on the nature of the sources themselves. For example, the absorption detected in the only–hard subsample is already well in excess of $N_H = 10^{22}\ \mathrm{cm}^{-2}$. If the intrinsic absorption is rapidly increasing with decreasing flux, as predicted by some AGN synthesis models (see Gilli, Salvati & Hasinger 2001), then the expected count rate of most of these hard sources can be much lower than the expected average $\simeq 1.3 \times 10^{-5}$ cts/s and they could be undetectable in the soft band down to fluxes as low as $S \simeq 10^{-19}$ erg s^{-1} cm^{-2}.

We have now about 80 redshifts for a subsample of sources (see Paper II, Rosati et al. 2001, Giacconi et al. 2001b, Hasinger et al. 2001b). We computed luminosities in the rest–

frame soft band after assuming an average power law spectrum with $\Gamma = 1.4$, in a critical universe with $H_0 = 50$ km/s/Mpc. The distribution of luminosities emitted in the soft band with redshift is shown in Figure 10 of Paper II. Most of the sources with $HR > 0$ appear to fall in the $L_{hard} = 10^{42} - 10^{44}$ erg s^{-1} range and are identified with TypeII absorbed AGNs. Data obtained with the HST observations of a small fraction of our field (Schreier et al. 2001) will address in detail the morphological properties of the optical counterparts. Softer sources with $HR < 0$ appear to span the range from 10^{40} to 10^{45} erg s^{-1}. At luminosities larger than 10^{42} erg s^{-1} these sources are mostly identified with TypeI AGN.

6 Sources in the CDFS, a closer view

In this section we will present in greater detail the properties of some sources in the CDFS. First, we show in Figure 11 the spectrum of a typical absorbed sources, one of the "blue dots" that appear in the color image with fluxes around $S \sim 10^{-14}$ erg s^{-1} cm^{-2}. This is an example of the relatively nearby ($z = 0.606$ in this case), absorbed sources that make up the hard X–ray background, solving the spectral paradox. The source has an hard X–ray luminosity of 3×10^{43} erg s^{-1}. If we fit the spectrum with an intrinsically absorbed power law, we find $\Gamma = 1.22 \pm 0.08$ with $N_H = (1.8 \pm 0.4)\ 10^{22}$ cm^{-2} (errors at 90% c.l.). We notice also a feature at the energy where the K_α Fe line complex is expected (about 4 keV).

At the low luminosity end, several sources are detected only in the soft band ($HR = -1$). Most of these objects are identified with galaxies at redshift less than 0.6, with soft luminosities restricted to a range between $L_x = 10^{40}$ erg s^{-1} and $L_x = 10^{42}$ erg s^{-1}. This population of relatively nearby galaxies with soft X–ray spectra has been found also by Hornschemeier et al. (2001) in the Chandra Deep Field North. In the plot S versus R, where S is the X–ray flux in the soft band (see Figure 12) this subsample appears to populate the low S/R region at fluxes $S < 10^{-15}$ erg s^{-1} cm^{-2}. We can use a criterium defined in the S–R plane to isolate this soft, low luminosity population of sources. If we define a subsample of sources detected only in the soft band, and optically extended (with a stellarity index less than 0.2 in the R–band image), we find 44 sources. The analysis of the stacked spectrum gives $\Gamma = 2.2 \pm 0.3$ with an upper limit for local absorption of $N_H = 10^{21}$ cm^{-2} (error and upper limit at 90% c.l.). If we repeat the fit with a Raymond–Smith spectrum, we find 3.4 ± 0.9 keV. These results are similar to that derived from the 300k sample (see Paper II) where we defined a subsample requiring $S/S_{opt} < 0.1$, $S_{tot} < 3 \times 10^{-15}$ erg s^{-1} cm^{-2}, and $HR < -0.5$. In this subsample, among the 18 sources selected in the low S/S_{opt} region, 10 have redshift, with an average value $\langle z \rangle = 0.25$. By visual inspection from the images in the R and B bands, at least 10 of these 18 sources appear clearly to be galaxies. If we fit their stacked spectrum with a power law, we find consistency with Galactic absorption, and a spectral slope $\Gamma = 2.0 \pm 0.2$ (90 % c.l.). If we repeat the fit with a thermal spectrum, we find a temperature of 3.5 ± 1.5 keV, which is too high to be produced by hot gas in the potential wells of galaxies. Such an apparent temperature may be due to the contribution of low–level nuclear activity or a population of low mass X–ray binaries. Both fits have a $\chi^2_\nu \simeq 1$. A better definition of the subsample will be available when the spectroscopic optical identification is completed.

Another important population of objects in the CDFS, despite its small solid angle, is consituted by groups and clusters of galaxies. The systematic search for extended sources is still ongoing. However, three extended sources at the level of $S \sim 1 - 3 \times 10^{-15}$ erg s^{-1} cm^{-2} are easily detected. We have redshift for the brightest cluster member of one of them ($z \sim 0.7$, see Figure 13), while the optical colors of the others are consistent with being moderate redshift clusters. Assuming an average redshift of $z \sim 0.5$, we analyzed the stacked spectrum of the three extended sources. The total spectrum is well fitted by a Raymond–Smith thermal spectrum with temperature $kT = 1.7^{+0.6}_{-0.4}$ keV and a metallicity of $Z = 0.3 Z_\odot$ (see Figure 14). The luminosities

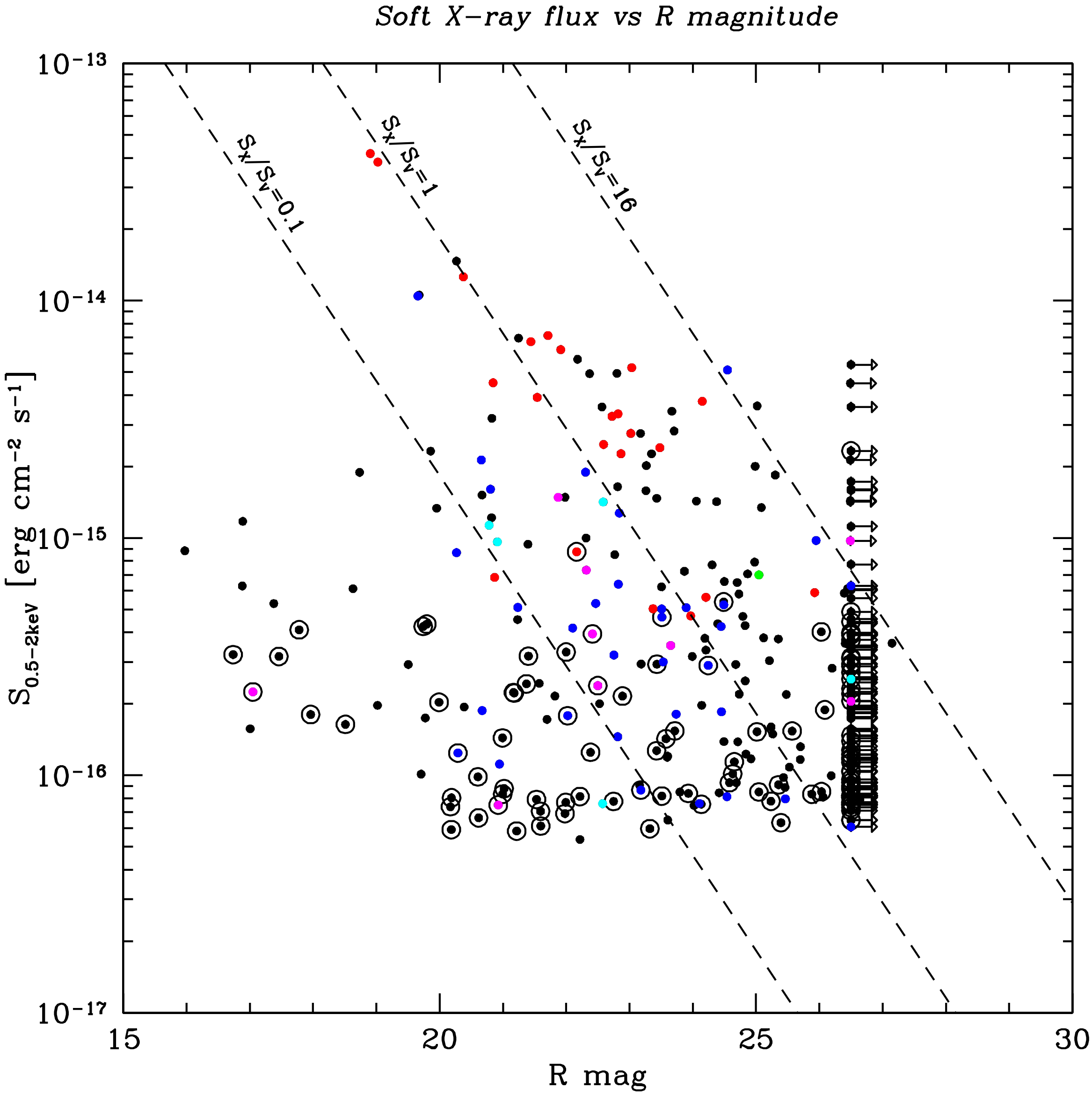

Figure 12: X–ray flux in the soft band versus optical R magnitude for Chandra sources. The dotted circles correspond to sources detected only in the soft band. Dashed lines correspond to constant X–ray to optical flux ratio of 1/10, 1, and 16 from left to right. For the objects without optical counterpart, we put a 3σ lower limit to the magnitude (arrows). Our spectral analysis allowed to identify some objects as TypeI AGNs (red dots), TypeII AGNs (blue dots) or normal galaxies (magenta dots). Note that below $S = 10^{-15}$ erg s^{-1} cm^{-2}, some sources depart more than three magnitudes from the $S_X/S_{opt} = 1$ relation.

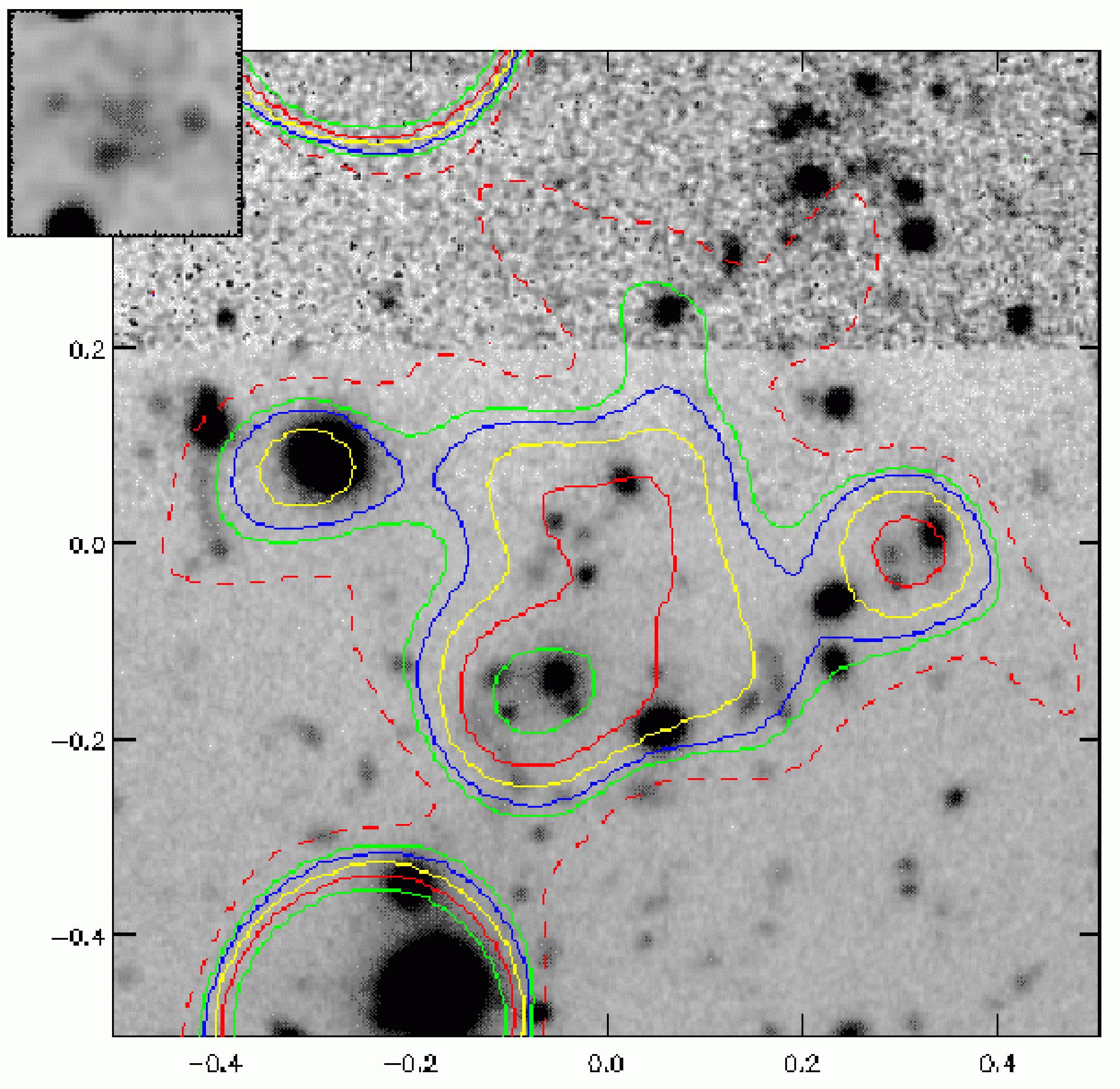

Figure 13: Optical image (R band) of the X–ray brightest group in the CDFS. The brightest cluster member is at redshift $z \sim 0.7$. The X–ray contours are at 2, 4, 5, 7 and 10 sigma above the background level. The X–ray soft image is shown in the inset (Giacconi et al. 2001b).

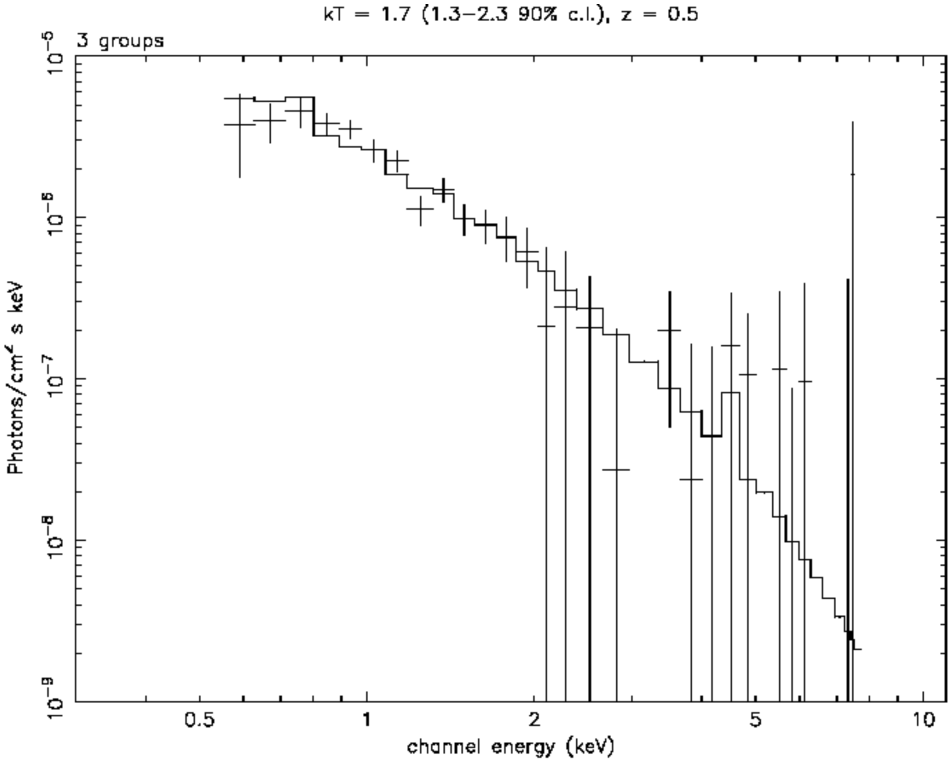

Figure 14: Stacked spectrum of the 3 brightest extended sources detected in the CDFS. The spectrum is well fitted by a thermal Raymond–Smith spectrum with $Z_{\odot} = 0.3$ (frozen) and $kT = 1.7^{+0.6}_{-0.4}$ keV.

are in the range $L \simeq 2 - 8 \times 10^{42}$ erg s^{-1} in the soft band. Therefore, these extended sources are consistent with the local L–T relation for groups, confirming the evidence for lack of evolution in the L–T relation (see Borgani et al. 2001).

Finally, we show an example of a Type II QSO, described in detail in Norman et al. (2001). Its optical spectrum shows narrow emission lines (Ly$_{\alpha}$, CIV, NV, HeII, OVI, O[III] and CIII]) that allow to estimate the redshift with good accuracy ($z = 3.700 \pm 0.005$), as shown in Figure 15. In the X–ray spectrum (with about 130 net counts) a prominent feature is detected at the 2 sigma level at the energy where the K$_{\alpha}$ Fe line complex is expected (1.4 keV). The line has an equivalent width of about 1 keV. The source can be considered Compton thick and its spectrum is well fitted by a reflection model with a Gaussian line at the rest–frame energy of 6.4 keV. The source shows substantial absorption ($N_H > 10^{24} - 10^{25}$ cm^{-2}) also in the case of a fit with absorbed power law. The unabsorbed X–ray luminosity is $L \simeq 10^{45\pm0.5}$ erg s^{-1}. The contribution of these highly absorbed objects to the hard XRB is expected to be relevant ($\simeq 30\%$), and most of them are expected to be at redshift $z = 1 - 2$, with a significant tail at higher redshifts (see Norman et al. 2001).

7 Conclusions

In these proceedings we reviewed some of the results from the 1 Ms exposure of the CDFS. We detected 360 sources down to a flux limit of 5×10^{-17} erg s^{-1} cm^{-2} in the 0.5–2 keV soft band and 4×10^{-16} erg s^{-1} cm^{-2} in the 2–10 keV hard band. For the hard counts we find evidence for flattening below $S \simeq 8 \times 10^{-15}$ erg s^{-1} cm^{-2}: at the faint end the differential counts are well fitted by a power law with a slope $\alpha_{diff} = 1.58 \pm 0.12$ (1 sigma error). After the inclusion of the ASCA sources at the bright end, the total contribution to the resolved hard X–ray background down to our flux limit now amounts to $(1.56 \pm 0.16) \times 10^{-11}$ erg cm^{-2} s^{-1} deg^{-2}. The uncertainty

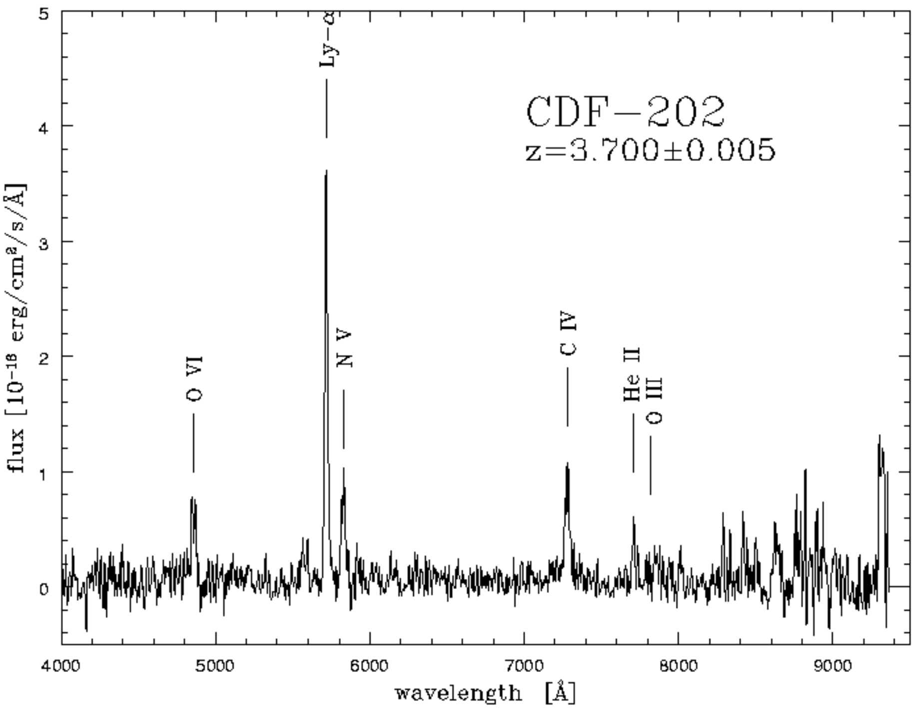

Figure 15: Optical spectrum of the QSO II found in the CDFS (Norman et al. 2001).

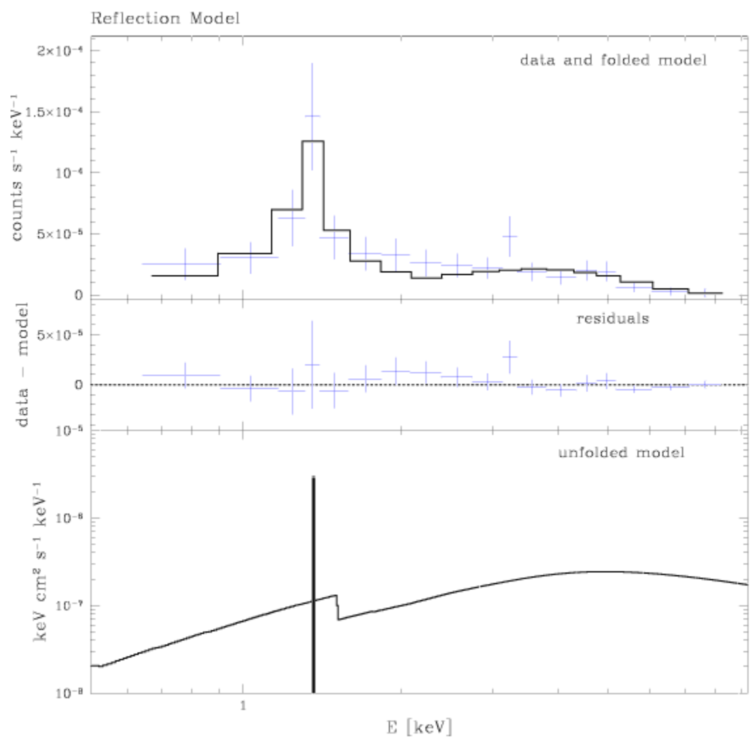

Figure 16: X–ray spectrum of the QSO II in the CDFS with reflection fit plus the Fe K line (Norman et al. 2001).

includes the variation of the average spectral slope in the hard sample, which can be as low as $\Gamma = 1.05$ for our faintest sources. With this new data we resolve $65 - 98\%$ of the hard XRB, given the uncertainties in the unresolved value, which ranges from 1.6 to 2.4×10^{-11} erg s^{-1} cm^{-2} deg^{-2}. The general properties of the X–ray background are now well established. The so called "spectral paradox" is solved by a hard, faint population of sources constituted mostly by nearby ($z \leq 1$) absorbed (Type II) AGN with luminosities $L \simeq 10^{42} - 10^{44}$ erg s^{-1}.

We confirm our previous finding on the average spectrum of the sources of the total sample, which can be well approximated with a power law with index $\Gamma = 1.375 \pm 0.015$. We also find a progressive hardening of the sources at lower fluxes, both for the soft and the hard samples. In particular, we divided the hard sample into four subsamples: bright ($S > 2 \times 10^{-14}$ erg s^{-1} cm^{-2}), medium ($2 \times 10^{-14} > S > 6 \times 10^{-15}$ erg s^{-1} cm^{-2}), faint ($S < 6 \times 10^{-15}$ erg s^{-1} cm^{-2}), and very faint ($S < 2 \times 10^{-15}$ erg s^{-1} cm^{-2}). The average power law is $\Gamma = 1.68 \pm 0.03$ for the bright subsample, $\Gamma = 1.42 \pm 0.03$ for the medium subsample, $\Gamma = 1.10 \pm 0.03$ for the faint subsample, $\Gamma = 1.05 \pm 0.05$ for the very faint subsample. The progressive hardening at faint fluxes is probably due to a stronger intrinsic absorption.

In the soft band the differential number counts show a slope $\alpha = 0.5 \pm 0.1$ for fluxes below 10^{-15} erg s^{-1} cm^{-2}. The soft X–ray background in the energy range 1–2 keV is now resolved at the level of 83–99% depending on the assumed value for the unresolved soft XRB.

We have also measured redshifts for $\simeq 80$ sources (see Paper II). The spectra will be presented in the catalog paper of the 1Ms exposure (Giacconi et al. 2001b) and described in a dedicated paper (Hasinger et al. 2001b). We find that the hard sources with $HR > 0$ are typically found at $z < 1$, with intrinsic luminosities between 10^{42} and 10^{44} erg s^{-1} in the soft band. Between the objects producing the 2–10 keV X–ray background, the ones with $HR > 0$ (producing 20–30% of the total XRB) appear relatively nearby (redshifts $z < 1$) and are most easily identified with Seyfert II galaxies (see also Barger et al. 2001).

In addition to the hard, faint AGNs that saturate the hard XRB, we find other interesting populations of sources in the CDFS. The observation at $S < 10^{-15}$ erg s^{-1} cm^{-2} of very soft ($HR < -0.5$) objects with L_X between 10^{40} and 10^{42} erg s^{-1} up to $z \simeq 0.3$ opens up a new window to the study of the evolution of galaxies at moderate z. A large number of galaxies could increase the number counts at low fluxes without contributing significantly to the XRB.

We presented also the spectral analysis of the three brightest extended sources detected in the CDFS. They are associated with moderate redshift groups of galaxies ($z \simeq 0.5 - 0.7$) and their average spectrum is well fitted by a Raymond–Smith model with an average temperature of $kT = 1.7 \pm 0.4$ keV.

Another important finding of Chandra is the detection of an obscured QSOs. A X–ray luminous, strongly absorbed source with a TypeII optical spectrum has been found at redshift $z = 3.7$. This source shows the most distant Fe K_α line detected so far, and it is extensively described in Norman et al. (2001). When the optical identification program will be completed, it will be possible to test whether the population of aborbed AGN is as large as assumed in the AGN synthesis models of the XRB (Madau, Ghisellini & Fabian 1993; Comastri et al. 1995; Gilli et al. 2001).

Acknowledgments

We thank Richard Bouwens for providing the modified version of Sextractor used for detection and Roberto Della Ceca for useful comments. P.T. acknowledge support from the *Training and Mobility of Researchers Programme* in order to attend the XXXVIth Rencontres de Moriond.

References

1. Barger, A. J., Cowie, L. L., Mushotzky, R. F., Richards, E. A. 2001, AJ, 121, 662
2. Bertin, E., Arnouts, S. 1996, A&A Supplement, 117, 393
3. Borgani, S., Rosati, P., Tozzi, P., Stanford, S.A., Eisenhardt, P.E., Lidman, C., Holden, B., Della Ceca, R., Norman, C., & Squires, G. 2001, ApJ submitted.
4. Brandt, W.N., et al. 2000, AJ, 119, 2349
5. Comastri, A., Setti, G., Zamorani, G., & Hasinger, G. 1995 A& A, 296, 1
6. Della Ceca, R., Castelli, G., Braito, V., Cagnoni, I. & Maccacaro, T. 1999a, ApJ, 524, 674
7. Della Ceca, R., Braito, V., Cagnoni, I. & Maccacaro, T. 1999b, astro-ph/0007430
8. Freeman, P.E., Kashyap, V., Rosner, R., & Lamb, D.Q. 2001, ApJ submitted
9. Garmire, et al. 2001, in preparation
10. Gendreau, K.C., et al. 1995 Publ. Astron. Soc. Jpn. 47, L5-L9
11. Giacconi, R., Rosati, P., Tozzi, P., et al. 2001, ApJ, 551, 624 (Paper I)
12. Giacconi, et al. 2001b, ApJ in preparation
13. Gilli, R., Salvati, M., & Hasinger, G. 2001, A&A, 366, 407
14. Giommi, P., Perri, M., Fiore, F. 2000, A&A, 362, 799
15. Hasinger, G., Burg, R., Giacconi, R., Hartner, G., Schmidt, J., Truemper, J., & Zamorani, G. 1993, A&A 275, 1
16. Hasinger, G., Burg, R., Giacconi, R., Schmidt, J., Truemper, J., & Zamorani, G. 1998, A&A 329, 482
17. Hasinger, G., et al. 2001a, A&A 365, L45
18. Hasinger, G., et al. 2001b, in preparation
19. Hornschemeier, A.E., et al. 2000, ApJ, 541, 49
20. Hornschemeier, A.E., et al. 2001, astro-ph/0101494
21. Ishisaki, Y., Makishima, K., Takahashi, T., Ueda, Y., Ogasaka, Y., & Inoue, H. 1999, ApJ submitted
22. Madau, P., Ghisellini G., & Fabian, A. C. 1993, ApJ, 410, L7
23. Marshall, F. et al. 1980, ApJ, 235, 4
24. Mushotzky, R.F., Cowie, L.L., Barger, A.J., & Arnaud, K.A. 2000, Nature, 404, 459
25. Norman, C., et al. 2001, ApJ submitted, astro-ph/0103198
26. Rosati, P., Della Ceca, R., Burg, R., Norman, C., Giacconi, R. 1995, ApJL, 445, 11
27. Rosati, P., et al. 2001, in preparation
28. Schreier, E., et al. 2001, ApJ, in press, astro-ph/0105271
29. Stern, D., et al. 2001, in preparation
30. Tozzi, P., et al. 2001, ApJ submitted (Paper II), astro-ph/0103014
31. Ueda, Y., et al. 1999, ApJ, 518, 656
32. Vecchi, A., Molendi, S., Guainazzi, M., Fiore, F., & Parmar, A.N. 1999, A&A, 349, 73
33. Wise, M. W., Davis, J. E. , Huenemoerder, D. P. , Houck, J. C. and Dewey, D. 2000, MARX technical manual, http://space.mit.edu/ASC/MARX/manual/manual.html